Wu Xiao
Dalian University of Technology
Room D-405
Chemical Engineering Lab Building of Western New Campus
No.2 Linggong Road
Dalian, P.R. China 116024
86-13500772096 fax: 86-411-84986291
wuxiao@dlut.edu.cn

July 14, 2022

Dear Prof. Editor:
I am pleased to submit an original research article entitled “A Partial Element Stage Cut Electrochemical Hydrogen Pump Model for Hydrogen Separation and Compression” by Wu Xiao et al. for consideration for publication in “AIChE Journal”.

In this work, a partial element stage cut electrochemical hydrogen pump (EHP) model for multiple H_2-contaning gases separation and hydrogen compression which embed real factors was established to study EHP performance accurately under whole hydrogen concentration. The accuracy and reliability of proposed model were verified from different aspects under four feedstock systems (H_2/N_2, H_2/CH_4, H_2/He and H_2/CO_2). Simulation results show that high hydrogen back-diffusion ratio can cause low energy efficiency under high cathode pressure and low feedstock hydrogen content. The variation law of hydrogen purity under multi-operating conditions was also studied, which shows dual-effect (GDL mass transfer and PEM resistance) can affect hydrogen purity prominently through current density under low feedstock hydrogen content and applied potential.

I would like to declare on behalf of my co-authors that the work described was original research that has not been published previously, and not under consideration for publication elsewhere, in whole or in part. All the authors listed have approved the manuscript that is enclosed. No conflict of interest exits in the submission of this manuscript, and manuscript is approved by all authors for publication.

We deeply appreciate your consideration of our manuscript, and we look forward to receiving comments from the reviewers.

Yours sincerely,
Wu Xiao
Associate Professor, Department of Chemical Engineering
Dalian University of Technology, China
E-mail: wuxiao@dlut.edu.cn;

Graphical Abstract：

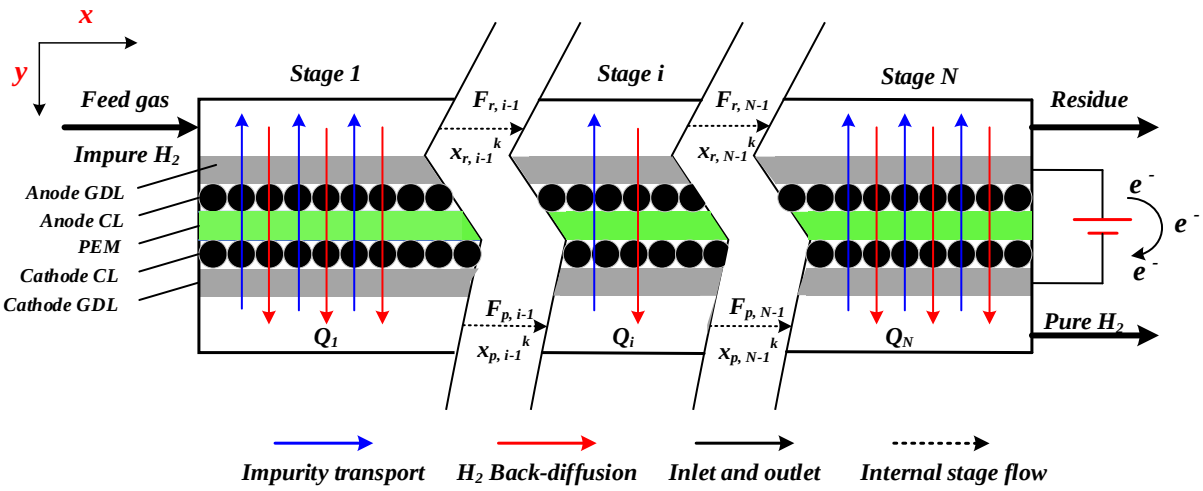

Research Highlights:

(1) A electrochemical hydrogen pump (EHP) model which based on partial stage cut method are proposed.

(2) Four real factors are introduced in the model to describe EHP performance accurately.

(3) The acuracy of EHP model is verified based on different aspects under four different feedstock systems.

(4) The variation law of current density caused by GDL mass transfer and PEM resistance are simulated and analyzed quantitatively.

(5) The back-diffusion behavior of hydrogen under cathode pressurization are simulated and analyzed quantitatively.

A Partial Element Stage Cut Electrochemical Hydrogen Pump Model for Hydrogen Separation and Compression

Andi Cheng[a], Wu Xiao[a,*], Xiaobin Jiang[a], Xuehua Ruan[a], Gaohong He[a], Xiangcun Li[a], Hanli Wang[b], Xuemei Wu[a,*]

[a] State Key Laboratory of Fine Chemicals, School of Chemical Engineering, Dalian University of Technology, 2 Linggong Road, Dalian, LN 116024, China;

[b] Dongyue R & D Center of Dongyue Group Ltd., State Key Laboratory of Fluorinated Functional Membrane Materials, Shandong Huaxia Shenzhou New Material Co., Ltd., Shandong, China

Corresponding author. E-mail address: wuxiao@dlut.edu.cn (W. Xiao); xuemeiw@dlut.edu.cn (X-M. Wu).

Abstract: In this work, a partial element stage cut electrochemical hydrogen pump (EHP) model for multiple H_2-contaning gases separation and hydrogen compression which embed real factors (anode impurity diffusion, hydrogen back-diffusion and anode catalyst deactivation) was established to study EHP performance accurately under full hydrogen concentration. The accuracy and reliability of proposed model were verified from four aspects (current density distribution, polarization curve, hydrogen recovery and purity) under different feedstock systems and wide pressure range. The model has good applicability and accuracy ($R^2 \geq 0.96$, simulation and experiment results comparison). Simulation results show that high hydrogen back-diffusion ratio can cause low energy efficiency under high cathode pressure and low feedstock hydrogen content. The variation law of hydrogen purity under multi-operating conditions was studied, which shows dual-effect (PEM and GDL resistance) can affect hydrogen purity prominently through current density under low feedstock hydrogen content and applied potential.

Keywords: Electrochemical hydrogen pump; Partial stage cut; Mathematical model; Hydrogen separation; Compression

1. Introduction

Hydrogen (H_2) is an important energy carrier. Due to its high heat value (1.2×10^5 kJ/kg), combustion products are non-pollution (only water) and can be transported through existing pipelines.[1] It is considered to a clean energy with the most development potential in 21st century. However, different with fossil energy (coal, petroleum and natural gas), hydrogen is not a primary energy. It must be produced by other energy, which can be stored in form of chemical energy and used in some way (fuel cell or combustion). No matter how hydrogen is obtained, separation is an eternal topic. On the one hand, over 90% hydrogen comes from fossil fuels and industrial by-product (a minor amount of hydrogen from bio-processes)[2,3], which contains impurities or by-products (CO, CO_2 and N_2 etc.) brought from raw materials or reaction process.[4,5] In the process of chemical-electrical energy conversion under catalyst, hydrogen purity will affect fuel cell performance[6] and service life directly.[7] Besides, due to the difference between hydrogen consumption and production end, hydrogen produced from renewable energy (solar and wind) needs to be transported through the existing natural gas pipeline network.[8] Although this transportation method reduces cost, but the efficient separation of hydrogen (H_2/CH_4) with pressure swing adsorption (PSA)[9,10] is difficult to achieve since low hydrogen content (10 - 30 mol%).[11] On the other hands, since the low specific volumetric energy density at atmospheric pressure, pressurized storage for hydrogen is necessary. Different kinds of gases have different compression work, due to the high initial specific volumes of hydrogen (11.11 Nm^3/kg).[12] Hydrogen requires about 9 times energy compared with methane and 15 times energy compared with air according to the adiabatic compression formula under the ideal condition of ignoring additional loss, which requires high compression power undoubtedly.[13] In summary, efficient hydrogen separation and compression must be considered to realize "hydrogen economy" in the future.

Electrochemical hydrogen pump (EHP) is also called electrochemical hydrogen compressor (EHC), which integrates hydrogen purification and compression functions. Providing a new way for hydrogen the efficient utilization. With its advantages, a host of scholars have studied EHP operation performance in detail. Lee et al.[14] recovered hydrogen from $H_2/N_2/CO_2$ mixture by EHP, which showed that higher temperature could improve EHP energy efficiency and product hydrogen purity. But higher inlet pressure can lead to greater impurity diffusion flux and decrease product hydrogen purity. Onda et al.[15] separated hydrogen from H_2/N_2 mixture and used a modified fuel

cell (FC) model[16] to forecast EHP performance. Experiment results showed that EHP could separate low content hydrogen from FC exhaust gas. Subsequently, Onda et al.[18] separated hydrogen from low hydrogen concentration mixture. Experiment results showed that EHP effective processing concentration ranged from 1 mol% to 99.99 mol%, which confirmed the full hydrogen concentration applicability of EHP. Abdulla et al.[19] investigated the H_2/CO_2 separation performance of EHP, which showed that energy efficiency was limited by hydrogen mass transport in gas diffusion layer (GDL) and multistage EHP with programmed applied potential profile (from high to low) could achieve more than 90% energy efficiency and 98% hydrogen recovery. Thomassen et al.[20] used high temperature (≥100 °C) EHP to separate hydrogen from H_2/N_2 and reformate gas (CO, CO_2 and CH_4) mixture, which showed the good dynamic response and low energy consumption. Schorer et al.[21] demonstrated that the biggest advantage of EHP was to realize the simultaneous separation and compression of hydrogen through the research of MEMPHYS project, which will make the storage and transportation of hydrogen more convenient.

Previous experiment studies on EHP hydrogen separation and compression performance have been abundant. However, there are few reports on EHP mathematical modeling method under multi-feedstock system and cathode high pressurization. Ibeh et al.[9] separated hydrogen from H_2/CH_4 and H_2/Ar mixtures and developed a simple differential equation model to forecast EHP performance. Nordio et al.[22] investigated the separation properties of EHP for H_2/CH_4, H_2/N_2 and H_2/He mixtures. A 1D + 1D model which solved by MATLAB® was developed to compare hydrogen separation and compression performance with pressure swing adsorption (PSA), which showed EHP was convenient under small scale and high outlet hydrogen pressure field. Danilov et al.[23] proposed a high temperature proton exchange membrane electrochemical hydrogen pump (HT-EHP) tanks-in-series mathematical model[45] based on mass and charge balance equations. Predicted polarization curve was consisted with the experiment data of Thomassen et al.[20] Toghyani et al.[24] established a three-dimensional numerical model based on finite volume method solved by ANSYS Fluent®, which showed that hydrogen exergy loss decreased 53% when GDL thickness decreased from 0.5 mm to 0.2 mm at current density of 5000 A/m^2.

In summary, mathematical model is the core of quantitative analysis of EHP hydrogen production process. Although previous scholars have developed a few mathematical models, which simulation data can consistent with the experiment data.

However, there are still some problems in the current EHP model, which undoubtedly restricts the further industrialized development of EHP. On the one hand, EHP also has the problem of cathode hydrogen back-diffusion like hydrogen fuel cell anode hydrogen crossover[25,26]and anode impurities diffusion that detrimental for EHP energy efficiency and product hydrogen purity, which strongly depending on the PEM properties and electrochemical reaction. Although Truc et al.[27] and Baik et al.[28] proposed hydrogen crossover numerical model based on membrane water content and temperature. But here lack of appropriate embedding methods for real factors. On the other hands, EHP anode catalyst undergoes reverse water gas shift reaction (RWGS) to generate CO under the CO_2-containing feedstock condition,[29] which occupies the anode catalyst active site, results the decrease of anode catalyst activity and EHP performance.[29] However, there is no EHP mathematical model for CO_2-containing feedstock condition based on strict RWGS kinetic equation. In summary, current EHP mathematical model lacks proper description of hydrogen back diffusion, anode impurity transmembrane transportation and anode catalyst deactivation. Existing algebraic and differential equation methods lack appropriate real factor embedding method, which need to be improved.

In view of the above problems, a partial element stage cut EHP mathematical model for hydrogen separation and compression which embed three real factors (anode impurity diffusion, hydrogen back-diffusion and anode catalyst deactivation) was established to predict EHP performance accurately. The accuracy and reliability of proposed model were verified from four aspects (current density distribution, polarization curve, cathode hydrogen yield and purity) under four different feedstock systems (H_2/N_2, H_2/CH_4, H_2/He and H_2/CO_2) and wide cathode pressure (0.1 - 1 MPa) to ensure accuracy. The EHP model will provide an important basis for its process simulation and optimization, and the study of hydrogen separation performance provides guidance for EHP industrialization application.

2. Mathematical model of electrochemical hydrogen pump

The working principle of EHP is shown in Figure 1, which is formed of anode and cathode gas diffusion layers (GDL), gas flow channel, catalyst layer (CL) and proton exchange membrane (PEM).[14] The core part of EHP is called membrane electrode assembly (MEA).[17] EHP working process can be described as a series of nine transport and reaction steps:[19]

(1) Anode hydrogen molecules (H_2) are transported across the anode GDL from anode gas flow channel to the anode CL.

(2) Hydrogen molecules are adsorbed on the anode CL.

(3) Adsorbed hydrogen molecules are oxidized to protons (H^+) and electrons(e^-).

(4) Electrons move from anode GDL to cathode GDL through external circuit.

(5) Protons move from the anode CL into and across the PEM.

(6) Protons adsorb onto the cathode CL.

(7) Protons and electrons combine adsorbed protons at the cathode CL.

(8) Protons recombine and desorb as hydrogen molecules from the cathode CL.

(9) Hydrogen gas molecules are transported across the cathode GDL to the cathode gas flow channel.

The whole process can be summarized by two electrochemical half-reactions and one total reaction as shown in Eqs. (1) - (3):

Anode hydrogen oxidation reaction (HOR):

$$H_2(P_a) \rightarrow 2H^+ + 2e^- \quad (1)$$

Cathode hydrogen evolution reaction (HER):

$$2H^+ + 2e^- \rightarrow H_2(P_c) \quad (2)$$

EHP overall reaction equation:

$$H_2(P_a) \rightarrow H_2(P_c) \quad (3)$$

Like the multistage equilibrium calculation of distillation column, partial element stage cut numerical technique can make simulation process efficient and convenient. Besides, this approach can also embed a variety of real factors to make simulation results accurate.[33] Some scholars have used this method to simulate gas membrane separation process. Coker et al.[31] proposed a membrane module model based on partial element stage cut method, which treat membrane module as several cells. Each cell's residue is fed to the next cell, and the permeate flow of the cell is a combination of local membrane permeation and the permeate flow from the next and previous cell. Katoh et al.[48] proposed a membrane module mathematical model considering nonideal mixing based on partial element stage cut method, which provided a reliable unsteady-state behaviors examination method for hollow fiber membrane gas separation modules. Chen et al.[32] proposed a dual-membrane module model based on partial element stage cut method, which has good applicability for H_2/CO_2 separation and can be established in natural gas[46] and oilfield associated gas[47] treatment simulation environment. Gilassi

et al.[33] used partial element stage cut method to realized hollow fiber membrane module modeling, which was suitable for natural gas and air separation simulation in Aspen Plus®. Therefore, the effectiveness of modeling method based on element stage cut method is proved, which provided sufficient theoretical basis.

Similar with membrane modules and fuel cell, EHP also has long gas flow channel, and its main purpose is to realize the separation of hydrogen and other components. However, although PEM has high selectivity, but it cannot prevent transmembrane behavior of other impurities. The specific modeling method of transmembrane behavior has not been mentioned in previous studies. In addition, the Nernst potential in the electrode along the gas flow channel is different since the hydrogen content decreases with the direction of the flow channel.[15,16] Simple algebraic equations[19] based on modification of Faraday's law cannot achieve the internal operating parameters (current density distribution, Nernst potential and overpotential distribution and H_2 mass transport limited current density, etc.) of the EHP. Although computational fluid dynamics (CFD) model can realize the visualization of EHP internal process,[24] but its computational resources cost is high, which scalability is limited. Therefore, it is necessary to use more effective partial element stage cut method to realize EHP modeling.

2.1. Model description

A partial element stage cut method which embed three kind of real factors is introduced here for EHP modeling to forecast hydrogen recovery rate, purity and other internal operating parameters. The H_2-containing gas enters from the anode, and the hydrogen reaches CL through GDL, which is dissociated into protons and electrons under external electric field. Single straight flow channel assumption is adopted here to not only deal with EHP gas flow channel with straight, Z pattern and serpentine but also can be used to large-scale EHP stack while occupying fewer time and resources. The cathode conditions (except cathode pressure P_c) are neglected here since it does not limit EHP performance. Because EHP has large aspect ratio (small hydraulics diameter D_H and large length $L_{channel}$). Therefore, the whole EHP anode part can be simplified as a series of continuous small block, which is similar with plug flow reactor.[45] Hydrogen transportation behavior in x-direction and y-direction can be purely considered as 1 - D and axial diffusion in the gas flow channel is ignored. Whole model can be simplified

as a half EHP model as shown in Figure 2.

(1) Hydrogen transport in GDL only considers diffusion.[38]

(2) Since the anode gas pressure is low (≤ 600 kPa) and temperature is low (20 - 120 ℃), all gases processed by EHP are considered as ideal mixture.

(3) EHP operation process can be regarded as isothermal[24] and steady state.

(4) Perfectly humidified PEM with no water clogging, constant membrane resistance.[35]

(5) Gas viscosity can be considered constant even anode hydrogen is entirely consumed.

(6) A plane catalyst layer (CL) is considered at the anode meaning that the electrochemical reaction takes place homogenously throughout the CL thickness.

(7) The aspect ratio and flow channel cross-sectional area have little effect on cell performance.[34,35] Similarly, the gas flow channel can be simplified as single straight flow channel, which no bending.

2.2. Model general equations

Like the oxygen transportation process in the cathode gas flow channel of hydrogen fuel cell,[38] based on the previous assumptions, steady state hydrogen transport equation in the anode gas flow channel is as follows:

$$\frac{\partial C_a(x,y)}{\partial x} = \frac{D^e}{u_a h_d} \cdot \frac{\partial C_G(x,y)}{\partial y}\Big|_{y=0} \tag{4}$$

where C_a is the hydrogen mole concentration in anode gas flow channel; C_G is the mole concentration of hydrogen in the GDL; u_a is the anode gas velocity; h_d is the gas diffusion layer thickness; D^e is the hydrogen effective diffusion coefficient in anode GDL, which can be calculated by Bruggeman correction, which can be expressed as follow:[36,37]

$$D^e = \frac{\varepsilon^\tau (1-s)^\tau (1-x_a^a)}{\sum_{b,b\neq a} \frac{x_a^b}{D_{a,b}}} \tag{5}$$

where ε and τ are the porosity and tortuosity, which detail data is from Chen et al.[37]; s is the liquid saturation; x_a is the mole fraction of hydrogen in gas flow channel, which are described in detail below; $D_{a,b}$ is the binary diffusivity of hydrogen and other component (a means H_2, b means other component), which can be calculated by Fuller - Schettler - Gidding equation:

$$D_{a,b} = \frac{10^{-3}T^{1.75}(\frac{M_a + M_b}{M_a M_b})^{0.5}}{P_a[(\sum V)_a^{\frac{1}{3}} + (\sum V)_b^{\frac{1}{3}}]^2} \quad (6)$$

where T is the operating temperature; M_a and M_b are the molecular weight of component a and b (a means hydrogen, b means other components); P_a is the anode pressure; $\sum V$ is the molecular diffusion volume, which are shown in Table 1.

The pressure drop in the anode gas flow channel is calculated by Hagen-Poiseuille equation [36] with channel size correction, which is shown in Eq. (7):

$$\frac{dP_a}{dx} = (55 + 41.5e^{\left(\frac{-3.4}{\frac{w_{channel}}{h_{channel}}}\right)}) \times \frac{\mu_{mix} u_a}{2D_H} \quad (7)$$

where $w_{channel}$ and $h_{channel}$ are the gas flow channel width and height; u_a is the flow channel gas velocity, which is assumed to be constant and calculated by Eq. (8) based on feedstock volume flow V_F; μ_{mix} is gas mixture viscosity, which also assumed to be constant and calculated by Unisim Design® based on Peng-Robinson fluid package for convenience; D_H is the hydraulic diameter,[36] which is calculated as Eq. (9):

$$u_a = \frac{V_F}{0.785 D_H^2} \quad (8)$$

$$D_H = \frac{2 w_{channel} h_{channel}}{h_{channel} + w_{channel}} \quad (9)$$

The steady state hydrogen diffusion equation in GDL is given as:

$$\frac{\partial^2 C_G(x,y)}{\partial y^2} = 0 \quad (10)$$

As the hydrogen content decreases along the gas flow channel, Nernst potential and overpotential are also changed. Anode and cathode charge balance equations are defined as:

$$C_{DL}^a \frac{d\eta_a(x)}{dt} = j_{EHP}(x) - j_a(x) \quad (11)$$

$$C_{DL}^c \frac{d\eta_c(x)}{dt} = -j_{EHP}(x) - j_c(x) \quad (12)$$

where $\eta_a(x), \eta_c(x)$ are non-ohmic overpotential of anode and cathode, respectively; C_{DL}^a, C_{DL}^c are double layer capacitances, respectively; $j_{EHP}(x)$ is the EHP current density along x, respectively; $j_a(x), j_c(x)$ are current density along x of anode and cathode, respectively.

Under steady-state conditions, EHP operating parameters are independent of time. Therefore, Eq. (11) and Eq. (12) can be simplified as:

$$\frac{d\eta_a(x)}{dt} = \frac{d\eta_c(x)}{dt} = 0 \tag{13}$$

$$j_{EHP}(x) = j_a(x) = |j_c(x)| \tag{14}$$

According to Butler - Volmer equation, the current density equations of anode and cathode are as follows:[23,40]

$$j_a(x) = \theta_H^2 j_0^a e^{\left[-\frac{E_A^a}{RT}\left(1-\frac{T}{T_{ref}}\right)\right]}\left[\frac{C_{cat,a}(x)}{C_{ref}}\right]^{0.5}\left[e^{\left(\frac{\alpha_a^a}{RT}\eta_a(x)\right)} - e^{\left(\frac{\alpha_c^a}{RT}\eta_a(x)\right)}\right] \tag{15}$$

$$j_c(x) = j_0^c e^{\left[-\frac{E_A^c}{RT}\left(1-\frac{T}{T_{ref}}\right)\right]}\left[\frac{C_{cat,c}(x)}{C_{ref}}\right]^{0.5}\left[e^{\left(\frac{\alpha_a^c}{RT}\eta_c(x)\right)} - e^{\left(\frac{\alpha_c^c}{RT}\eta_c(x)\right)}\right] \tag{16}$$

where θ_H is the effective surface coverage for HOR (surface coverage values are derived from the RWGS kinetic equation solving results) from 0 - 1; E_A^a, E_A^c are the activation energy of HOR and HER (while a and c means anode and cathode); *T* is the operating temperature; *R* is the ideal gas constant; j_0^a, j_0^c are the exchange current density of HOR and HER; $\alpha_a^a, \alpha_c^a, \alpha_a^c$ and α_c^c are the charge transfer coefficients of anode and cathode electrochemical reactions; $C_{cat,a}(x), C_{cat,c}(x)$ are the hydrogen concentration of the CL surface; C_{ref} is the reference hydrogen concentration which equals to feedstock hydrogen concentration; T_{ref} is the electrochemical reactions reference temperature. Electrochemical kinetic parameters are shown in Table 2.

According to Eq. (15) and Eq. (16), the current densities of anode and cathode are equal under steady-state. The influence of cathode conditions except pressure on EHP can be ignored. Only anode current density needs to be calculated. The overpotential value reflects the electrochemical reaction rate, which is related to the value of Nernst potential, anode current density and PEM resistance:

$$\eta_a(x) = [E - E_N(x) - j_a(x) \cdot r] \times op \tag{17}$$

$$E_N(x) = \frac{RT}{ZF} ln[\frac{P_c x_c^1(x)}{P_a x_a^1(x)}] \tag{18}$$

where *E* is applied potential provided by power source; *r* is the PEM resistance; $E_N(x)$ is the Nernst potential, which is related to the partial pressure of anode hydrogen; *Z* is the number of transferred charges; *F* is the Faraday constant (96485 C/mol); Hao et al.[39] used hydrogen reference electrode to investigate EHP reaction mechanism, which shown that anode overpotential accounts for about 0.25 of the overall overpotential in the cell average current density range of 7 - 80 mA/cm^2. When the current density is greater than 700 mA/cm^2, the value of *op* is about 1 according the extrapolation results.

2.3. RWGS kinetic equation

Carbon dioxide at the anode can undergo reverse water gas shift reaction (RWGS) under electric field, which total reaction is shown in Eq. (19) with the adsorbed hydrogen on the CL, which generate adsorbed CO that can poison catalyst. Gu et al.[41] used strip cyclic voltammetry (CV) to investigate the RWGS in Pt and Pt/Ru alloy catalysts of PEMFC. The CO equilibrium concentration were consistent with kinetic equation calculation results.[42,43] Nordio et al.[30] proved that RWGS is the main reason of EHP performance degradation, the inactivation of the catalyst is faster at 22.5 ℃ compared with 19 ℃ since RWGS is an endothermic reaction. Danilov et al.[23] used empirical correlation for carbon monoxide surface coverage given by Rodrigues et al.[44] to predict the high temperature EHP catalyst performance. In this work, the novel strategy based on RWGS kinetic equation Eqs. (19) - (25)[41-43] is used to realize the accurate forecast for EHP operation performance in CO_2-containing feedstock.

$$CO_2 + H_2 \leftrightarrow CO + H_2O \tag{19}$$

Although total RWGS can be simply written as shown in Eq. (19). But the actual reaction route is complicated, which can be divided into six steps:

$$CO - Cat \overset{k_1,k_{-1}}{\Longleftrightarrow} CO + Cat \tag{20}$$

$$H_2O + Cat \overset{k_2,k_{-2}}{\Longleftrightarrow} H_2O - Cat \tag{21}$$

$$H_2O - Cat \overset{k_3,k_{-3}}{\Longleftrightarrow} HO - Cat + H^+ + e^- \tag{22}$$

$$CO_2 + H^+ + e^- + 2Cat \overset{k_4,k_{-4}}{\Longleftrightarrow} CO - Cat + HO - Cat \tag{23}$$

$$H_2 + 2Cat \overset{k_5,k_{-5}}{\Longleftrightarrow} 2Cat - H \tag{24}$$

$$Cat - H \overset{k_6,k_{-6}}{\Longleftrightarrow} H^+ + e^- + Cat \tag{25}$$

The change of surface coverage θ of different species can be expressed as follows:

$$\rho \frac{d\theta_H}{dt} = 2r_5 - 2r_{-5} - r_6 + r_{-6} \tag{26}$$

$$\rho \frac{d\theta_{H_2O}}{dt} = r_2 - r_{-2} - r_3 + r_{-3} \tag{27}$$

$$\rho \frac{d\theta_{OH}}{dt} = r_3 - r_{-3} + r_4 + r_{-4} \tag{28}$$

$$\rho \frac{d\theta_{CO}}{dt} = r_4 - 2r_{-4} - r_1 + r_{-1} \tag{29}$$

The surface coverage of each species (H, H_2O, OH and CO) does not change with time under steady state. The normalization equation of surface coverage is shown in Eq. (30).

$$\theta_0 + \theta_H + \theta_{H_2O} + \theta_{OH} + \theta_{CO} = 1 \tag{30}$$

The detailed kinetic expression data are shown in Table A1 and Table A2. By solving the above Eqs. (26) - (30) and Eqs. (A1) - (A3), the catalyst surface coverage data can be obtained to realize the correction of current density calculation Eq. (15). The accuracy of the calculation method is verified below.

2.4. Partial cut stage strategy for model solution

Eqs. (4) - (10) descripted the hydrogen transportation and diffusion action in gas flow channel and GDL. The boundary conditions of them are shown in Eqs. (31) - (32). Feedstock pressure and flow rate also belong to boundary conditions, which will be given in the model verification and analysis part.

$$C_G(x, y = 0) = C_a(x) \tag{31}$$

$$-D^e \frac{\partial C_G(x,y)}{\partial y}|_{y=h_d} = \frac{j_a(x)}{ZF} \tag{32}$$

According to above boundary conditions, the hydrogen concentration relationship of adjacent stage in anode gas flow channel can be expressed as Eq. (33):

$$C_a^{i+1} = C_a^i - \frac{j_{a,i}\Delta x}{ZFu_a h_{channel}} \tag{33}$$

The hydrogen concentration at the interface between CL and GDL has the following relationship in Eq. (34):

$$C_G(x, y = h_d) = C_{cat,a}(x) \tag{34}$$

Therefore, the relationship between C_c and $C_{cat,a}$ in *i* stage can be established:

$$C_{cat,a}^i = C_a^i - \frac{h_d j_{a,i}}{ZFD_i^e} \tag{35}$$

where *i* is the stage number; C_a^i, $C_{cat,a}^i$ are the hydrogen concentrations in CL and GDL of stage i, respectively; $j_{a,i}$ is the anode stage current density; Δx is the step size equal to $L_{channel}/N$, where $L_{channel}$ is the channel length, N is the total stage number.

All key variables varying with the flow channel direction are discretized, and the detailed parameters of each stage can be solved. Once current density is solved, other parameters (recovery rate, energy efficiency, stage compositions, purity etc.) can be achieved naturally.

$$P_{a,i} = P_{a,in} - (55 + 41.5e^{\left(\frac{-3.4}{\frac{W_{channel}}{h_{channel}}}\right)}) \times \frac{\mu_{mix} u_a \Delta x(i-1)}{2D_H} \tag{36}$$

$$E_{N\,i} = \frac{RT}{ZF} \ln[\frac{P_c x_{c,i-1}^1}{P_{a,i-1} x_{a,i-1}^1}] \tag{37}$$

$$\eta_{a,i} = [E - E_{N,i-1} - j_{a,i-1} \cdot r] \times op \tag{38}$$

$$D_i^e = \frac{\varepsilon^\tau (1-s)^\tau (1 - x_{a,i-1}^{k=1})}{\sum_{k=1,k\neq 1} \frac{x_{a,i-1}^{k\neq 1}}{D_{k=1,k\neq 1}}} \tag{39}$$

$$j_{a,i} = \theta_{H,i}^2 j_0^a e^{\left[-\frac{E_A^a}{RT}\left(1-\frac{T}{T_{ref}}\right)\right]} [\frac{C_{cat,a}^i}{C_{ref}}]^{0.5} \left[e^{\left(\frac{\alpha_a^a}{RT}\eta_{a,i}\right)} - e^{\left(\frac{\alpha_c^a}{RT}\eta_{a,i}\right)}\right] \tag{40}$$

Based on Eqs. (31)-(40), the current density $j_{a,i}$ of stage i can be obtained. EHP average current density can be expressed as Eq. (41):

$$I_{EHP} = \frac{\Delta x}{L_{channel}} \sum_{i=1}^{N} j_{a,i} \tag{41}$$

2.5. Gas molecule transmembrane diffusion

Due to the partial pressure difference on both sides of the PEM, anode impurities and cathode hydrogen can transport across the PEM. In order to predict the transmembrane behavior of gas molecules accurately, a gas transmembrane calculation strategy based partial element stage cut method is used in this model. Whole model principle and solution strategy are shown in Figure 3.

The component permeability and mass balance equations of stage *i* are as follows:

$$Q_i^k = \begin{cases} \frac{k_k(\frac{A}{N})(P_{a,i}x_{a,i-1}^k - P_c x_{c,i-1}^k)}{l_m}, k \neq 1 \\ -\frac{k_k(\frac{A}{N})(P_c x_{c,i-1}^k - P_{a,i}x_{a,i-1}^k)}{l_m}, k = 1 \end{cases} \tag{42}$$

$$Q_i = \sum_{k=1}^{n} Q_i^k \tag{43}$$

$$F_{a,i-1}x_{a,i-1}^k + F_{c,i-1}x_{c,i-1}^k = F_{a,i}x_{a,i}^k + F_{c,i}x_{c,i}^k \tag{44}$$

$$F_{a,i-1}x_{a,i-1}^k + Q_i^{k=1} = F_{a,i}x_{a,i}^k + \frac{j_{a,i}}{ZF} + \sum_{k=2}^{n} Q_i^k \tag{45}$$

$$F_{c,i-1}x_{c,i-1}^k + \sum_{k=2}^{n} Q_i^k = F_{c,i}x_{c,i}^k + \frac{j_{a,i}}{ZF} + Q_i^{k=1} \tag{46}$$

where k_k is the component permeability; A is the MEA area; $P_{a,i}$ is the anode stage pressure; P_c is the cathode pressure which is constant; $x_{a,i}^k$ and $x_{c,i}^k$ are anode and cathode stage component mole fraction; Q_i^k is the stage permeation mole flowrate of component k; Q_i is the stage net permeation mole flowrate; $F_{a,i}$ and $F_{c,i}$ are stage total mole flowrate; k is the component number (k=1 means hydrogen, k>1 means other

components, n is the number of components, $k \in [1, n]$); l_m is the PEM thickness.

3. Model solution and validation

3.1. Model solution

Since PEM has high selectivity, which only passes protons nearly. Therefore, the initial impurities content of the first stage (i=1) on the cathode side is set as 0. The PEM permeability data of different gas molecules are used for model solving process, and the barrier effect of GDL and CL are ignored. Solution procedures are shown in Figure 4.

3.2.Model validation

In order to verify the model effectiveness under different feedstock and cathode pressure, four feedstock systems with typical industrial application background (H_2/N_2, H_2/CH_4, H_2/He and H_2/CO_2) are used to verify the accuracy of the model. The model is verified from four aspects: current density distribution, polarization curve under different cathode pressure, hydrogen recovery rate and purity to ensure the accuracy. The basic parameters required for model validation are shown in Table 3. The comparison of simulation and experiment results are shown in Table B1, B2, B3 and B4.

3.2.1. H_2/N_2 system

According to the experiment results of Onda et al.[15,16,18] and Nordio et al, [22] the effectiveness of EHP is verified from the views of polarization curve and current density distribution. As shown in Figure 5(a-b), the polarization curve is consistence with experiment data in wide hydrogen feedstock content under two different experiment and operating conditions (average relative error: 7.69%; feedstock hydrogen content: 1 - 99 mol%). As shown in Figure 6, the EHP current density distribution have a good agreement with experiment data under different applied potential (average relative error is 1.39% to 9.93% when the average current density increases from 20 mA/cm^2 to 40 mA/cm^2). Above experiment and simulation comparation results show that proposed model can be used to the prediction of EHP performance in H_2/N_2 feedstock system, and has full concentration applicability for H_2-containing gases.

3.2.2. H_2/CH_4 and H_2/He systems

As shown in Figure 7(a-b), the simulation polarization curves have a good agreement (relative error: 2.27%, 2.32%) with the experiment data under different feedstock hydrogen content and large average current density range, which shows the effectiveness of proposed model under H_2/CH_4 and H_2/He feedstock systems. The obvious turning point between PEM membrane resistance control to hydrogen mass transport control can be seen in Figure 7(a-b) under low feedstock hydrogen content (20 mol%), which means the hydrogen mass transport and current density calculation strategy are correct. Proposed model can be used in the EHP performance prediction under H_2/CH_4 and H_2/He feedstock systems. As shown in Figure 8, the simulation values of hydrogen recovery rate are also consistent with the experiment data. Proposed EHP model can be used in the hydrogen recovery rate prediction.

3.2.3. H_2/CO_2 system

Due to the negative effect of RWGS on EHP anode CL, the EHP performance under CO_2-containing environment will be inhibited, which means EHP in CO_2-containing feedstock system has lower current density under the same applied potential compared with other systems.

According to the experiment results of Abdulla et al.[19], the effectiveness of EHP in H_2/CO_2 feedstock condition is verified from the views of polarization curve. As shown in Figure 9, the simulation polarization curves have a good agreement with the experiment data in different feedstock hydrogen content, which means the model has a good capability under CO_2-containing environment. Besides, the anode CL coverage prediction method based on the detailed RWGS kinetic method is accurate.

As shown in Figure 10, the simulation average current density curves based on different feedstock hydrogen content have a good agreement with the experiment data. Although hydrogen mass transport rate is fast, which means small mass transfer resistance and hydrogen at CL can be consumed rapidly, which means the current density initially increases linearly with hydrogen content at constant applied potential. As the feedstock hydrogen content increases, the hydrogen content at CL cannot be consumed completely, which results the current density reaches limiting value like a horizontal level. Increasing applied potential (100 - 300 mV) can make the limiting current density jump to a high level (175 - 525 mA/cm^2). Such simulation results are

consistent with the experiment results completely. In summary, the effectiveness of mass transfer solving strategy and RWGS kinetics under CO_2-containing feedstock system are verified. Proposed model is applicable to the prediction of EHP performance under H_2/CO_2 feedstock system.

3.2.4. Hydrogen purity and cathode compression

The simulation results under different feedstock conditions and operating parameters are consistent with the experiment data, which proves the effectiveness of the developed EHP model. However, there is no experiment-simulation comparative study on EHP hydrogen purification and compression performance. In order to explore EHP hydrogen purification and compression performance furtherly, the effectiveness of proposed model is verified from the view of purity curve and cathode pressured polarization curve according to the experiment results of Nordio et al.[22,30], Onda et al.[15] and Strobel et al.[49] according to Table 4 and Table 5.

As shown in Figure 11(a-b), the simulation purity curves are consistence with experiment data, which means the stage permeation flow calculation strategy is corrected. As shown in Figure 11(a), the hydrogen purity increases with the feedstock hydrogen content under the same applied potential, which means low feedstock hydrogen content results high transmembrane pressure difference. According to the Eq. (42), more impurities can reach to cathode, which results low hydrogen purity.

Besides, the hydrogen purity also increases with the applied potential as shown in Figure 11(a-b), which means high applied potential results high stage current density. According to Faraday's law, higher current density will result higher hydrogen production, which dilute impurities to improve hydrogen purity.

As shown in Figure 12(a), the polarizations curves under cathode pressurization are consistence with experiment data under the cathode pressure range of 0.1 - 1.0 MPa, which means the current density solving strategy have a wide cathode pressure applicability. Although a large deviation between simulation and experiment values can be seen in Figure 12(b), which may be caused by the large deviation between simulation and experiment parameters. Based on this result, we can use this model to study the integrated performance of hydrogen separation and compression in the performance study part.

4. Performance study based on simulation

In order to explore the hydrogen separation and compression performance of EHP under different feedstock and operation conditions furtherly. In this section, we will study the EHP performance from two aspects: operating conditions (operating temperature, anode feedstock pressure, feedstock hydrogen content and cathode pressure) and PEM properties (gas permeability and membrane resistance). H_2/CH_4 (Hydrogen mixed natural gas separation) and H_2/CO_2 (reforming and biomass gasification H_2-containing gases) which have typical industrial application background are selected as the target analyze systems.

4.1.Electrochemical reaction properties

In order to study the electrochemical reaction and mass transfer characteristics of EHP furtherly, the EHP polarization curves under different temperatures based on the model calculation are given as shown in Figure 13 (a-b). At a lower voltage, the polarizations show linear. PEM resistance is the main limiting factor. Increasing applied potential can improve average current density then increase hydrogen production. When the voltage continues to increase, the average current density reaches to hydrogen transport limiting current density and GDL mass transport resistance become the main limiting factor, which is similar with the behavior of high temperature catalyst in gas-solid heterogeneous catalytic reaction and consistence with the experiment results of Abdulla et al.[19] Besides, higher polarization curve slope can be seen in Figure 13(b), which causes by RWGS under CO_2-containing feedstock. On the whole, higher operating temperature can increase current density when applied potential in relatively low ($\leqslant$500 mV). However, relative high temperature can result in low current density under high applied potential ($\geqslant$700 mV), which means the blocking effect lead by GDL mass transport resistance play a significant role. In summary, the applied potential at turning point is optimal for max hydrogen production and low energy consumption. Appropriate applied potential need to be considered comprehensively during EHP design and working.

As shown in Figure 14 (a-b), hydrogen mass transport limiting current density deceases with the increase of operating temperature, which caused by the rapid consumption of reactant along with the anode gas flow channel under higher operating temperature. HOR on catalyst surface has low activation energy[40] (34.6 kJ/mol), which

means the electrochemical reaction equilibrium concentration of hydrogen on the catalyst surface is equal to the real concentration of hydrogen. Hydrogen concentration difference between GDL and CL is the main limiting factor under this condition. Although GDL effective diffusion coefficient D^e increases with the increase of temperature, but the bigger hydrogen concentration difference between gas flow channel and CL caused by rapid consumption of hydrogen results greater blocking effect, which leads to a decrease in hydrogen transport limiting current density with temperature.

Besides, hydrogen mass transfer limiting current density at the same temperature increases with the feedstock hydrogen content (50 - 80 mol%) according to Figure 14 (a-b), which shows that higher feedstock hydrogen content can relieve the blocking effect caused by rapid consumption of hydrogen to meet the demand of catalyst under the same operating temperature. Although RWGS can curb anode catalyst performance under CO_2-containing feedstock condition, but the limiting current density between CO_2 and no-CO_2 feedstock condition hardly changes as shown in Figure 14 (a-b), which shows that hydrogen transport limited current density is an intrinsic property, which only related to feedstock hydrogen content and operating temperature. The inhibition effect of catalyst caused by RWGS only affects the energy consumption reaching to hydrogen transport limiting current density.

4.2.Hydrogen recovery rate and energy efficiency

Hydrogen recovery rate reflects the hydrogen separation capacity, and the energy efficiency reflects the relationship between the separation capacity and energy consumption, which mathematical relationships are shown in Eqs. (47) - (48).

$$\mathrm{H_2\ Recovery\ rate}\ (RE, \%) = \frac{F_{c,N} x_{c,N}^1}{F_{in} x_{in}^1} \times 100\% \quad (47)$$

$$\mathrm{Energy\ efficiency}\ (EE, \%) = \frac{RE \cdot F_{in} x_{in}^1 \Delta H_{combustion} - I_{EHP} AE}{F_{in} x_{in}^1 \Delta H_{combustion}} \times 100\% \quad (48)$$

where superscript 1 means H_2 is the target component; $\Delta H_{combustion}$ is the combustion heat of hydrogen (286 kJ/mol); E is the applied potential; F_{in} and $F_{p,N}$ are anode feedstock mole flow and cathode outlet mole flow, respectively; x_{in}^1 and $x_{p,N}^1$ are hydrogen mole contents of the anode feedstock and cathode outlet, respectively. I_{EHP} is the average current density; A is the MEA area; RE is the hydrogen recovery rate.

As shown in Figure 15(a) and (c), the hydrogen recovery rate increases with

applied potential and then reaches to constant level, which means current density reaches to hydrogen mass transport limiting value and hardly changes. Max hydrogen recovery rate under hydrogen mass transport control decreases with the increase of feedstock hydrogen content (H_2 content: 20 - 80 mol%), which from 64% to 43% and 63% to 39%, respectively. Although RWGS under CO_2-containing feedstock can curb CL performance that higher applied potential need to be adopted to achieve same hydrogen recovery rate, but the max recovery rate hardly changes, which means the hydrogen transport limiting current density related with max hydrogen recovery rate is an intrinsic property and independent of catalyst. But energy efficiency under CO_2-containing feedstock is 48%, 34% and 21%, respectively, lower than no-CO_2 feedstock (53%, 43% and 25%), which means higher electric energy need to be consumed to overcome the detrimental effect caused by CO poisoning. Energy efficiency peak value decreases from 53% to 25% and 48% to 21% respectively as shown in Figure 15(b) and (d), which means more hydrogen lost in anode residue with the increases of feedstock hydrogen content. In summary, the turning point between PEM resistance and GDL mass transport control is the best operating point that best energy utilization and hydrogen recovery can be achieved.

The relationship between hydrogen recovery rate, applied potential and energy efficiency under cathode high pressure (20 MPa) are similar with the cathode low pressure (0.13 MPa) as shown in Figure 16(a-d). As shown in Figure 16 (a) and (c), hydrogen recovery rate under different feedstock nearly same with the cathode low pressure, but the energy efficiency peak value decreases a lot, which from 53%, 43% and 25% to 45%, 36% and 22%. The absolute difference of energy efficiency peak value (H_2/CH_4) under different cathode pressure is 8%, 7% and 3%, respectively, which can be seen that energy efficiency peak value difference (3%) under 80 mol% feedstock hydrogen content is much lower than 20 mol% feedstock hydrogen content (8%). Besides, obvious energy efficiency curve crossing can be seen in Figure 16(b) and (d). Higher feedstock hydrogen content (80 mol%) shows higher energy efficiency compared with low feedstock hydrogen content (20 mol%) under relatively lower hydrogen recovery rate($\leqslant$50%). Improving that high cathode pressure (20 MPa) may causes a reverse effect compared with low cathode pressure, hydrogen back-diffusion need to be analysis under hydrogen cathode pressure.

In order to achieve quantitative analysis of cathode hydrogen back-diffusion behavior precisely, the hydrogen back-diffusion ratio expression is given as shown in

519 Eq. (49):

$$\mathrm{H_2\ Back-diffusion\ ratio\ (\%)} = \frac{\sum_{i=1}^{N} Q_i^1}{F_{in} x_{in}^1} \times 100\% \quad (49)$$

520 where Q_i^1 is the hydrogen back-diffusion mole flow in stage i; x_{in}^1 is the feedstock
521 hydrogen mole fraction; F_{in} is the feedstock mole flow.

522 As shown in Figure 17(a-b), the quantitative relationship between hydrogen back-
523 diffusion rate and applied potential can be seen directly. Back-diffusion rate under low
524 hydrogen feedstock content (20 mol%) is 4 times than high hydrogen feedstock content
525 (80 mol%), which is corresponding to the Eq. (42) that high transmembrane pressure
526 difference results more hydrogen diffusion flow. Besides, from the view of membrane
527 material, the new membrane materials with anti-diffusion function to decrease
528 membrane permeability can curb this phenomenon, which requires more scholars to
529 conduct membrane research furtherly.
530

531 **4.3.Hydrogen purity**

532 Due to the existence of differential pressure on both sides of PEM, anode
533 impurities diffuse to cathode, resulting in impure hydrogen. Besides, the hydrogen
534 production process is affected by the current density directly, which means the hydrogen
535 yield follows Faraday's law. Hydrogen production and impurity permeate process can
536 affect hydrogen purity like a double-edged sword. Therefore, some operating
537 parameters (operating temperature, anode feedstock and cathode pressure) that can
538 affect current density need to be analysis here. In order to make the change of hydrogen
539 purity obviously, the impurity content (ppm, $1\ \mathrm{ppm} = 1 \times 10^{-6}$) is used in the figures.

540 As shown in Figure 18(a-d), the effects of feedstock pressure and operating
541 temperature on hydrogen purity is different with the feedstock hydrogen content.
542 Obvious boundary between PEM resistance and GDL hydrogen transport resistance
543 control can be seen in Figure 18(a). When operating temperature on the left of the
544 boundary, impurity content decreases with the operating temperature, which means that
545 PEM resistance is the main limiting factor. Once operating temperature over than
546 boundary, impurity content increases with the increase of the operating temperature,
547 which means that EHP operating point reaches to hydrogen mass transport control area.
548 Current density is limited by GDL mass resistance and decreases with the increase of
549 temperature, which decreases hydrogen production and results in low hydrogen purity.
550 With the increase of feedstock hydrogen content (40 - 60 mol%), the boundary between

PEM resistance and hydrogen transport resistance control disappear and PEM resistance become an only limiting factor as shown in Figure 18(b-d), higher operating temperature is good for increasing hydrogen purity.

Besides, hydrogen purity also increases with the increase of the feedstock hydrogen content, which lowest impurity content decreases from 1977 ppm to 924 ppm as shown in Figure 18(a-d). However, impurity content decreases with the increase of the feedstock pressure in Figure 18(c-d), which is abnormal according to Eq. (42). It is probably because the high feedstock pressure decreases Nernst potential according to Eq. (17) and Eq. (18), which increases current density and hydrogen purity under high hydrogen feedstock content (60 - 80 mol%).

With the increase of the cathode pressure (0.5 - 1 MPa), the lowest impurity content increases from 1977 ppm to 3930 ppm under feedstock hydrogen content is 20% as shown in Figure 18(a) and Figure 19(a). Impurity change trend under high hydrogen content (80 mol%) feedstock also shows the same behavior, which means that high cathode pressure can increase Nernst potential that causes lower current density and hydrogen production according to Eq. (17) and Eq. (18). Besides, the partial pressure difference hardly changes, which means the permeate flow of impurities hardly changes. Based on the joint action of two reasons, resulting the high impurity content under cathode high pressure.

As the core of EHP, PEM provides proton transport channel for electrochemical hydrogen separation process. In addition, gas molecules can also pass through PEM, which is related to PEM permeability. According to Eq. (42), the gas permeate flow increases with the differential pressure. As shown in Figure 20(a-b), the hydrogen purity increases with the permeability under the constant PEM resistance. However, PEM resistance also has a huge influence on hydrogen purity under constant permeability. Because low PEM resistance under constant operating applied potential means high current density, which results higher hydrogen production. Raising the applied potential (150 mV to 400 mV) can improve hydrogen purity under other operating conditions do not change, that the impurity content is decrease significantly. In summary, PEM with low gas permeability and resistance can improve hydrogen purity effectively.

5. Conclusions

In this work, a partial element stage cut electrochemical hydrogen pump (EHP) mathematical model which embed real factors (anode impurity diffusion, hydrogen back-diffusion and anode catalyst deactivation) was established to study EHP performance accurately. Then, four gas systems (H_2/N_2, H_2/CH_4, H_2/He and H_2/CO_2) were used to verify the effectiveness of the model. The simulation results of current density distribution, polarization curve, hydrogen purity and recovery rate are consistent with experiment data (polarization curve relative error: H_2/N_2: 7.69%; H_2/CH_4: 2.27%; H_2/He: 3.32%; H_2/CO_2: 5.00%), which verifies the effectiveness of the model.

Furtherly, H_2/CH_4 (hydrogen mixed natural gas) and H_2/CO_2 (biomass gasification and reforming gas) with typical industrial application background were selected as the target analysis system to study EHP performance (polarization, hydrogen recovery rate, energy efficiency and hydrogen purity). PEM resistance and GDL hydrogen transport resistance control area under different operating temperatures (25 - 90 mol°C) and feedstock hydrogen content (20 - 80 mol%) were determined. Increasing operating temperature can increase current density when EHP operating point in PEM resistance control area, but this behavior is contrary when operating point in GDL mass transfer resistance control area. RWGS can curb anode catalyst performance, but the limiting current density hardly changes, which demonstrated that the hydrogen transport limited current density is an intrinsic property Hydrogen recovery rate and energy efficiency analysis results show that high cathode pressure (20 MPa) can causes high hydrogen back-diffusion ratio (5.14%) than cathode low pressure (0.13 MPa), which results low energy efficiency under low hydrogen feedstock content (20 mol%). The variation law of hydrogen purity under multi-operating conditions (temperature, feedstock pressure and cathode pressure) was studied. Obvious boundary between PEM resistance and hydrogen transport resistance control can be seen under low hydrogen feedstock content (20 mol%) and applied potential (300 mV), which will disappear under high feedstock hydrogen content (80 mol%). Due to the existence of higher Nernst potential, hydrogen impurity content is higher under cathode high pressure (1 MPa, 2275 - 3930 ppm) compared with cathode low pressure (0.5 MPa, 924 - 1977 ppm). Besides, PEM with low gas permeability and resistance can improve hydrogen purity effectively.

In summary, this work provides a feasible prediction method for EHP performance from the perspective of mathematical model. In future works, the technical and

economic evaluation method based on proposed model for EHP hydrogen production process will be established to form a systematic EHP optimization design method.

Notation

*The variable unit in all tables used in calculation process are converted to international system of units (SI) according to the following table.

CL= Catalyst layer

EE= Energy efficiency

EHP= Electrochemical hydrogen pump

EHC= Electrochemical hydrogen compressor

GDL= Gas diffusion layers

HOR= Hydrogen oxidation reaction

HER= Hydrogen evolution reaction

MEA= Membrane electrode assembly

PEM= Proton exchange membrane

RWGS= Reverse water gas shift

A= MEA area, cm^2

C_a= Mole concentration of hydrogen in anode gas flow channel, mol/cm^3

C_G= Mole concentration of hydrogen in GDL, mol/cm^3

C_{cat}= Mole concentration of hydrogen in CL, mol/cm^3

C_{ref}= Reference hydrogen mole concentration, mol/cm^3

C_{DL}^a= Anode double layer capacitance, C/cm^2

C_{DL}^c= Cathode double layer capacitance, C/cm^2

D_H= Gas flow channel hydraulic diameter, cm

D^e= Effective diffusion coefficient in the GDL, cm^2/s

$D_{a,b}$= Gas binary diffusivity of hydrogen (a) and others component (b), cm^2/s

647 E= Applied potential, mV

648 E_N= Nernst potential, mV

649 F= Faraday's constant, 96485 C/mol

650 F_a= Anode mole flowrate, mol/s

651 F_c= Cathode mole flowrate, mol/s

652 $h_{channel}$= Gas flow channel height, cm

653 h_d= GDL thickness, cm

654 I_{EHP}= EHP average current density, mA/cm^2

655 j=Current density (including exchange current density j_0^a, stage current density $j_{a,i}$), mA/cm^2

656 k_k= PEM permeability, $\mathrm{mol}/(\mathrm{m}\cdot\mathrm{s}\cdot\mathrm{Pa})$

657 $L_{channel}$= Gas flow channel length, cm

658 l_m= PEM thickness, cm

659 M= Molecular weight, g/mol

660 N= Total stage cut numberop= Anode electrode overpotential/Total overpotential

661 Q= Gas diffusion flow rate, mol/s

662 P_a= Anode pressure, Pa

663 P_c= Cathode pressure, Pa

664 R= Ideal gas constant, $\mathrm{J}/(\mathrm{mol}\cdot\mathrm{K})$

665 r= PEM resistance, $\Omega\cdot\mathrm{cm}^2$

666 s= Liquid saturation

667 T= Operating temperature, K

668 T_{ref}= Electrochemical kinetic reference temperature, K

669 u_a= Gas flow channel velocity, cm/s

670 V_F= Feedstock gas volume flowrate, cm^3/s

671 $\sum V$= Molecule diffusion volume, cm^3/mol

672 $w_{channel}$= Gas flow channel width, cm

673 x_a= Mole flow channel of anode gas flow channel

674 x_c= Mole flow channel of cathode gas flow channel

675 Z= Charge transfer number

676

677 ## Greek letters

678 η= Anode and cathode overpotential, mV

679 ε= GDL porosity

680 τ= GDL tortuosity

681 μ= Gas mixture viscosity, Pa · s

682 α= Charge transfer coefficient

683 θ= CL surface coverage

684 δ= Relative deviation

685 Σ= Sum

686

687 ## Subscripts

688 a= Anode gas flow channel

689 $channel$= Anode gas flow channel

690 cat= Catalyst layer

691 c= Cathode gas flow channel

692 d= Gas diffusion layer

693 F= Feedstock

694 G= Gas diffusion layer

695 i= Stage number subscript ($i = 1, 2, 3 \ldots N-1, N$)

696 ii= Number of electrode reaction rate ($i = 3,4,6$)

697 mix= Gas mixture

698 m= Proton exchange membrane

699 n= Number of components

700 N= Nernst potential

701 ref= reference value

702 k= Component number subscript (k=1 means H_2)

Acknowledgments

We gratefully thank the financial support from National Key Research and Development Program of China (Grant No. 2019YFE0119200), Science Fund for Creative Research Groups of the National Natural Science Foundation of China (22021005), National Natural Science Foundation of China (22141001) and Key Research and Development Projects in Shandong Province (2022CXGC010303).

Credit authorship contribution statement

Andi Cheng: Conceptualization, Methodology, Writing - original draft, Wu Xiao: Conceptualization, Writing - review & editing, Supervision, Xiaobin Jiang: Formal analysis, Investigation, Gaohong He: Methodology, Formal analysis, Xiangcun Li: Formal analysis, Hanli Wang, Methodology, Xuemei Wu: Conceptualization, Supervision, Xuehua Ruan: Software, Validation.

Declaration of competing interest

The authors declare that they have no known competing financial interests or personal relationships that could have appeared to influence the work reported in this paper.

Literature Cited

1. Singla MK, Nijhawan P, Oberoi AS. Hydrogen fuel and fuel cell technology for cleaner future: A review. Environ Sci Pollut R. 2021; 28: 15607-15626.
2. Sikarwar VS., Zhao M, Clough P, Yao J, Zhong X, Memon MZ, Shah Nilay, Anthony JE, Fennell PS. An overview of advances in biomass gasification. Energy Environ Sci. 2016; 9: 2939.
3. Couto N, Monteiro E, Silva V, Rouboa A. Hydrogen-rich gas from gasification of Portuguese municipal solid wastes. Int J Hydrogen Energ. 2016; 41: 10619-10630.
4. Al-Rahbi AS, Williams PT. Hydrogen-rich syngas production and tar removal from biomass gasification using sacrificial tyre pyrolysis char. Appl Energ. 2017; 190: 501-509.
5. Secer A, Kucet N, Faki E, Hasanoqlu A. Comparison of coegasification efficiencies of coal, lignocellulosic biomass and biomass hydrolysate for high yield hydrogen production. Int J Hydrogen Energ. 2018; 43: 21269-21278.
6. Bernardo G, Araujo T, Silva Lopes T, Sousa J, Mendes A. Recent advances in membrane technologies for hydrogen purification. Int J Hydrogen Energ. 2020; 45: 7313-7338.
7. Rhandi M, Tregaro M, Dryart F, Deseure J, Chatnet M. Electrochemical hydrogen compression and purification versus competing technologies: Part I. Pros and cons. Chinese J Catal. 2020; 41: 756-769.

8. Ishaq H, Dincer I. Performance investigation of adding clean hydrogen to natural gas for better sustainability. J Nat Gas Sci Eng. 2020; 78: 103236.
9. Ibeh B, Gardnera C, Ternanb M. Separation of hydrogen from a hydrogen/methane mixture using a PEM fuel cell. Int J Hydrogen Energ. 2007; 32: 908-914.
10. Nordio M, Wassie SA, Annaland MVS, Tanaka DAP, Sole JLV, Gallucci F. Techno-economic evaluation on a hybrid technology for low hydrogen concentration separation and purification from natural gas grid. Int J Hydrogen Energ. 2020; 46: 23417-23435.
11. Dehdari L, Burgers I, Xiao P, Li KG, Singh R, Webley PA. Purification of hydrogen from natural gas/hydrogen pipeline mixtures. Sep Purif Technol. 2022; 282: 120094.
12. Midilli A, Ay M, Dincer I, Rosen MA. On hydrogen and hydrogen energy stratefies. I: current status and needs. Renew Sust Energ Rev. 2005; 9: 255-271.
13. Khaksarfard R, Kameshki MR, Paraschivoiu M. Numerical simulation of high pressure release and dispersion of hydrogen into air with real gas model. Shock Waves. 2010; 20: 205-216.
14. Lee HK, Choi HY, Choi KH, Park JH, Lee TH. Hydrogen separation using electrochemical method. J Power Sources. 2004; 132: 92-98.
15. Onda K, Ichihara K, Nagahama M, Minamoto Y, Araki T. Separation and compression characteristics of hydrogen by use of proton exchange membrane. J Power Sources. 2007; 164: 1-8.
16. Onda K, Araki T, Taniuchi T, Sunakawa D, Wakahara K, Nagahama M. Analysis of Current Distribution at PEFCs Using Measured Membrane Properties and Comparison with Measured Current Distribution. J Electrochem Soc. 2007; 154, 2: 247-257.
17. Casati C, Longhi P, Zanderighi L, Bianchi F. Some fundamental aspects in electrochemical hydrogen purification/compression. J Power Sources. 2008; 180: 103-113.
18. Onda K, Araki T, Ichihara K, Nagahama M. Treatment of low concentration hydrogen by electrochemical pump or proton exchange membrane fuel cell. J Power Sources. 2009; 188: 1-7.
19. Abdulla A, Laney K, Padilla M, Sundaresan S, Benziger J. Efficiency of Hydrogen Recovery from Reformate with a Polymer Electrolyte Hydrogen Pump. AIChE Journal. 2011; 57: 1767-1779.
20. Thomassen M, Sheridan E, Kvello J. Electrochemical hydrogen separation and compression using polybenzimidazole (PBI) fuel cell technology. J Nat Gas Sci Eng. 2010; 2: 229-234.
21. Schorer L, Schmitz S, Weber A. Membrane based purification of hydrogen system (MEMPHYS). Int J Hydrogen Energ. 2015; 44: 12708-12714.
22. Nordio M, Rizzi F, Manzolini G, Mulder M, Raymakers L, Annaland MVS, Gallucci F. Experiment and modelling study of an electrochemical hydrogen compressor. Chem Eng J. 2019; 369: 432-442.
23. Danilov VA, Kolb G, Cremers C. Tanks-in-series model for high-temperature electrochemical hydrogen pump. Int J Hydrogen Energ. 2021; 46: 11536-11543.
24. Toghyani S, Baniasadi E, Afshari E, Javani, N. Performance analysis and exergoeconomic assessment of a proton exchange membrane compressor for electrochemical hydrogen storage. Int J Hydrogen Energ. 2020; 45: 34993-35005.
25. Kocha SS, Yang JD, Yi JS. Characterization of Gas Crossover and Its Implications in PEM

Fuel Cells. AIChE Journal. 2006; 52: 1916-1925.
26. Brunetti A, Fontananova E, Donnadio A, Casciola M, Vona MLD, Sgreccia E, Drioli E, Barbieri G. New approach for the evaluation of membranes transport properties for polymer electrolyte membrane fuel cells. J Power Sources. 2012; 205: 222-230.
27. Truc NT, Ito S, Fushinobu K. Numerical and experiment investigation on the reactant gas crossover in a PEM fuel cell. Int J Heat Mass Tran. 2018; 127: 447-456.
28. Baik KD, Hong BK, Kim MS. Effects of operating parameters on hydrogen crossover rate through Nafion membranes in polymer electrolyte membrane fuel cells. Renew Energ. 2013; 57: 234-239.
29. Yan WM, Chu HS, Lu MX, Weng FB, Jung GB, Lee CY. Degradation of proton exchange membrane fuel cells due to CO and CO_2 poisoning. J Power Sources. 2012; 188: 141-147.
30. Nordio M, Barain ME, Raymakers L, Annaland MVS, Mulder M, Gallucci F. Effect of CO_2 on the performance of an electrochemical hydrogen compressor. Chem Eng J. 2020; 392: 123647.
31. Coker DT, Freeman BD. Modeling Multicomponent Gas Separation Using Hollow-Fiber Membrane Contactors. AIChE Journal. 1998; 44: 1289-1302.
32. Chen B, Ruan XH, Jiang XB, Xiao W, He GH. Dual-Membrane Module and Its Optimal Flow Pattern for H_2/CO_2 Separation. Ind Eng Chem Res. 2016; 55: 1064-1075.
33. Gilassi S, Taghavi SM, Rodrigue D, Kaliaguine S. Simulation of Gas Separation Using Partial Element Stage Cut Modeling of Hollow Fiber Membrane Modules. AIChE Journal. 2018; 64: 1766-1777.
34. Wang XD, Duan YY, Yan WM, Peng XF. Effects of flow channel geometry on cell performance for PEM fuel cells with parallel and interdigitated flow fields. Electrochim Acta. 2008; 53: 5334-5343.
35. Chevalier S, Josset C, Auvity B. Analytical solutions and dimensional analysis of pseudo 2D current density distribution model in PEM fuel cells. Renew Energ. 2018; 125: 738-746.
36. Jung SP, Lee CI, Chen CC. An efficient method for numerical predictions of the performance characteristics of fuel cells. I. Model development and validation. J Power Sources. 2012; 199: 179-194.
37. Chen Q, Niu ZQ, Li HK, Jiao K, Wang Y. Recent progress of gas diffusion layer in proton exchange membrane fuel cell: Two-phase flow and material properties. Int J Hydrogen Energ. 2021; 46: 8640-8671.
38. Bernardi DM, Verbrugge MW. Mathematical Model of a Gas Diffusion Electrode Bonded to a Polymer Electrolyte. AIChE Journal. 1991; 37: 1151-1163
39. Hao YM, Nakajima H, Inada A, Sasaki K, Ito K. Overpotentials and reaction mechanism in electrochemical hydrogen pumps. Electrochim Acta. 2019; 301: 274-283.
40. Song CJ, Tang YH, Zhang JL, Zhang JJ, Wang HJ, Shen J, McDermid S, Li J, Kozak P. PEM fuel cell reaction kinetics in the temperature range of 23-120 ℃. Electrochim Acta. 2003; 52: 2552-2561.
41. Gu T, Lee WK, Zee JWV. Quantifying the ‘reverse water gas shift’ reaction inside a PEM fuel cell. Appl Catal B Environ. 2003; 56: 43-49.
42. Springer TE, Rockward T, Zawodzinski T.A, Gottesfeld S. Improved optical model for thin film silicon solar cells. J Electrochem Soc. 2001; 148: 11.

43. Liu P. Logadottir A, Norskov JK. Modeling the electro-oxidation of CO and H_2/CO on Pt, Ru, PtRu and Pt_3Sn. Electrochim Acta. 2003; 48: 3731-3742.
44. Rodrigues A, Amphlett JC, Mann RF, Peppley BA, Roberge PR. Carbon monoxide poisoning of proton-exchange membrane fuel cells. In: IECEC-97 proceedings of the thirty-second intersociety energy conversion engineering conference (cat. No. 97CH6203). IEEE. 1997; 2: 768-773.
45. Saravanathamizhan R, Paranthaman R, Balasubramanian N. Tanks in Series Model for Continuous Stirred Tank Electrochemical Reactor. Ind Eng Chem Res. 2008; 47: 2976-2984.
46. Chen B, Ruan XH, Xiao W, Jiang XB, He GH. Synergy of CO_2 removal and light hydrocarbon recovery from oil-field associated gas by dual-membrane process. J Nat Gas Sci Eng. 2015; 26: 1254-1263.
47. Chen B, Jiang XB, Xiao W, Dong YN, Hamouti IE, He GH. Dual-membrane natural gas pretreatment process as CO_2 source for enhanced gas recovery with synergy hydrocarbon recovery. J Nat Gas Sci Eng. 2016; 34: 563-574.
48. Katoha T, Tokumura M, Yoshikawa H, Kawase Y. Dynamic simulation of multicomponent gas separation by hollow-fiber membrane module: Nonideal mixing flows in permeate and residue sides using the tanks-in-series model. Sep Purif Technol. 2011; 76: 362-372.
49. Strobel R, Oszcipok M, Fasil M, Rohland B, Jorissen L, Garche J. The compression of hydrogen in an electrochemical cell based on a PE fuel cell design. J Power Sources. 2002; 105: 208-215.

Appendix A: RWGS kinetic expressions and parameters

$k_3, k_{-3}, k_4, k_{-4}, k_6$ and k_{-6} are electrode reaction rate constants and affected by anode Nernst potential $E_{N,a}(x)$, which are shown as follows:

$$k_{ii} = k_{ii}^0 \exp[\frac{(1-\alpha_a^a)FE_{N,a}(x)}{RT}] \quad \text{(A1)}$$

$$k_{-ii} = k_{-ii}^0 \exp[\frac{-\alpha_a^a FE_{N,a}(x)}{RT}] \quad \text{(A2)}$$

$$E_{N\,a}(x) = \frac{RT}{ZF} \ln[\frac{101325}{P_{a,H_2}(x)}] \quad \text{(A3)}$$

where $ii = 3,4$ and 6; α_a^a is the anode charge transfer coefficient; F is the Faraday constant; R is the ideal gas constant; T is the EHP operating temperature; $P_{a,H_2}(x)$ is the anode gas flow channel pressure; $E_{N,a}(x)$ is the anode electrode Nernst potential.

Appendix B: Data comparison and error analysis

The simulation and experiment results of polarization curves and hydrogen impurity content under different systems are compared. The results are shown in Figure B1, B2, B3 and B4. The relative error of polarization curve under different feedstock systems is 7.69%, 2.27%, 3.32% and 5.00% respectively. All decisive indicators (R^2) of model verification in this work are greater than 0.96.